Microscopic Origins of the Long-Range Charge-Density Wave in Kagome FeGe

Saif Siddique, Mason Klemm, Qi Tang, Mehrdad T Kiani, Mostafa Hassani, Pengcheng Dai, Judy J Cha

Microscopy and Microanalysis, **31** (7), 2025, 660–663
https://doi.org/10.1093/mam/ozaf048.329

Microscopy AND Microanalysis

Proceedings

Microscopic Origins of the Long-Range Charge-Density Wave in Kagome FeGe

Saif Siddique[1,*], Mason Klemm[2], Qi Tang[3], Mehrdad T Kiani[1], Mostafa Hassani[1,3], Pengcheng Dai[2], and Judy J Cha[1]

[1]*Department of Materials Science and Engineering, Cornell University, Ithaca, NY, USA*
[2]*Department of Physics & Astronomy, Rice University, Houston, TX, USA*
[3]*Sibley School of Mechanical and Aerospace Engineering, Cornell University, Ithaca, NY, USA*
*Corresponding Author: ms2895@cornell.edu

Charge-density wave (CDW) is an electronic state characterized by modulations of the electron density and periodic lattice distortions [1]. Like other correlated electronic states, systems with CDWs exhibit strong electron-electron and electron-phonon interactions and hence CDW phases are often found near superconductivity and magnetism in the phase diagrams [2]. Studying CDWs is thus critical to understand the interplay between different correlated states and help reveal factors that govern the stability and transitions of these states. Recently, kagome-lattice FeGe (*B35* phase) has been shown to exhibit a CDW phase transition at $T_{CDW} \approx 100$ K, far below the antiferromagnetic (AFM) ordering temperature ($T_N \approx 410$ K) [3]. Not only is FeGe the first system to have CDW order within an AFM order, the onset of CDW enhances the AFM moment and induces an anomalous Hall effect, indicating CDW is closely intertwined with the magnetic order in FeGe. This observation, combined with the inherent geometric frustration and flat bands of the kagome lattice that results in non-trivial electronic behavior, makes FeGe a unique platform to explore novel correlated behaviors, including CDW.

At T_{CDW} ~100 K, FeGe undergoes a 2×2 CDW transition, where the Ge atoms in the Ge|Fe columns (Fig. 1a) are displaced to form dimers along the *c*-axis. The CDW is short-ranged with correlation lengths ranging between 3.3 nm – 4.5 nm [3]. Surprisingly, this CDW can be tuned by simple post-growth annealing [4-6]. For example, post-growth annealing of FeGe between 280-480°C, followed by quenching to room-temperature, can induce a long-range CDW, while annealing at 560°C and subsequent quenching suppresses the CDW altogether (Fig. 1b). We can cycle between the states repeatedly by annealing [5,6]. Concurrent with drastic changes to CDW order, different annealing conditions greatly affect the transport properties and magnetic order in FeGe. While this annealing-tunability of CDW has been demonstrated using transport measurements, scanning tunneling microscopy, and X-ray diffraction, a microscopic picture that explains this behavior is lacking. Here, we use electron diffraction, scanning transmission electron microscopy (STEM) techniques, and *in situ* mechanical indentation in a scanning electron microscope (SEM) to explore the microscopic origins of the long-range CDW in FeGe.

To study the annealing-dependence of CDW, we image two FeGe crystals annealed at 320°C and 560°C; the former shows a long-range CDW while the latter shows no CDW. The samples were prepared using a Thermo Fisher Scientific (TFS) Helios G4 UX focused-ion beam (FIB) and imaged using TFS Titan Themis and TFS Spectra 300 X-CFEG operated at 300 kV. Selected-area electron diffraction (SAED) patterns collected at 100 K in the [110] zone axis of FeGe, using a Gatan 636 cryo-TEM holder, show the expected sharp satellite peaks at $\mathbf{q} = (h + ½, k + ½)$ from long-range CDW in the 320°C annealed sample (Fig. 1c,d).

To investigate presence of any structural differences, we perform atomic-resolution STEM imaging using a high-angle annular dark-field (HAADF) detector at 100 K and construct an average image with two unit cells (Fig. 1e,f). Intensity line profiles reveal that in the sample without CDW (i.e. 560°C annealed sample), the intensity of Ge|Fe columns is lower than expected (Fig. 1g). While intensity differences in HAADF-STEM images can stem from various factors, we hypothesize that in this case, they are from Ge vacancies, induced by annealing. These vacancies lower the net atomic number (Z) of the column, thereby reducing the Z-contrast. We corroborate this hypothesis by performing *in situ* annealing of a long-range CDW sample using a DENSSolutions heating/biasing TEM holder. We collect energy-dispersive X-ray (EDX) spectra, which show that after annealing at 520°C, the Ge-Lα peak intensity is reduced (Fig. 1h,i; spectra are normalized to Fe-Lα peak). When reannealed at 320 °C, no change in the Ge-Lα peak intensity is observed. Careful post-annealing mass measurements also reveal a percentage mass loss ranging between 0.144 – 0.548% after a 560°C anneal, while no mass loss was observed after 320°C annealing. Given that Ge has a higher vapor pressure than Fe, this provides more evidence of presence of Ge vacancies in 560°C annealed samples. Since Ge atoms dimerize to form CDW, Ge vacancies prevent the formation of CDW.

To gain further insights into the structural differences of the two annealed samples, we use four-dimensional STEM (4D-STEM) at 100 K. Reconstructed bright-field STEM images from the 4D-STEM scans reveal the presence of extended defects exclusively in the 320°C annealed sample (Fig. 2a,b). The presence of these extended defects can help explain why this sample exhibits long-range CDW. These defects form from the precipitation of vacancies [7], leaving the Ge|Fe columns in regions away from defects free of vacancies. This allows the Ge atoms to dimerize and undergo the CDW transition. In contrast to this, the 560 °C annealed sample has uniformly distributed Ge vacancies preventing CDW formation, as evidenced by the absence of satellite peaks (Fig. 2d).

Interestingly, in the long-range CDW sample we observe stronger CDW satellite peaks near defects than away from them (Fig. 2c). Mapping the Bragg and CDW satellite peak intensities onto real-space shows that CDW is indeed stronger at the defects (Fig. 2e,f). This could suggest that the extended defects stabilize the CDW order. To test this, we induce extended defects in samples with short-range CDW (i.e., as-grown FeGe) and no CDW, and image them at 100 K to see if long-range CDW nucleates. We

perform *in situ* nanoindentation in a Zeiss LEO field-emission SEM using Alemnis Standard Assembly nanoindenter and a Berkovich tip (Fig. 3a,b) to introduce defects into the crystals. FIB is then used to prepare electron transparent samples from the indented region. To visualize lattice defects from the indentation, we image the samples using annular bright-field STEM (ABF-STEM, Fig. 3c,e). The SAED patterns at 100 K, however, do not show any satellite peaks, indicating that extended defects do not stabilize CDW.

In conclusion, by employing cryogenic-STEM and combining real and reciprocal space characterizations, we observed two types of defects in FeGe: Ge vacancies and extended defects. The presence of vacancies prevents Ge dimerization, thereby preventing the formation of long-range CDW. But extended defects absorb these vacancies, resulting in regions of stoichiometric FeGe, which can form long-range CDW. The ability to manipulate correlated states through annealing is also observed in other systems, such as copper oxide superconductors and van der Waals magnet [8,9]. Our findings help develop a microscopic understanding of how annealing affects the structure and influences the lattice, magnetic and charge correlations [10].

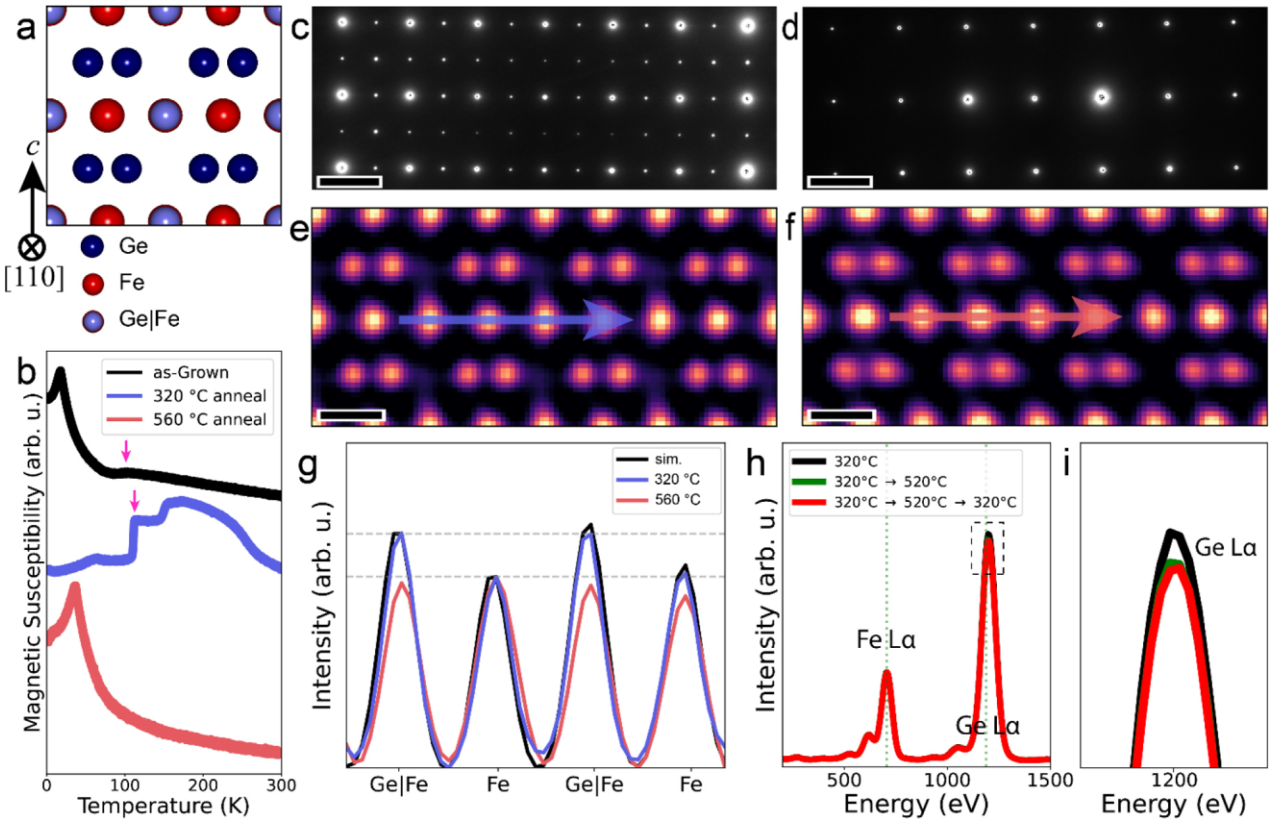

Figure 1: **a.** Atomic model of FeGe in its [110] zone-axis. The three different atomic columns are labeled. **b.** Magnetic susceptibility of the same sample after different annealing conditions. The CDW transitions in as-grown and 320 °C annealed samples are indicated by arrows. SAED patterns for **(c)** 320 °C and **(d)** 560 °C annealed samples at 100 K. Average HAADF-STEM images of the **(e)** 320 °C and **(f)** 560 °C annealed samples at 100 K. **g.** Intensity line profiles of the two samples compared with simulated intensities. The Ge|Fe column intensity in 560 °C annealed sample is lower than expected. **h.** EDX spectra of the same sample after *in situ* annealing showing a decrease in the Ge-Lα peak intensity. The spectra are normalized with respect to the Fe-Lα peak. **i.** Zoomed-in view of the Ge-Lα peak. The decrease in intensity in the Ge-Lα peak is ∼52 times greater than the noise level of the spectra. Scale bars for (**c, d**) = 2 nm^{-1}; for (**e, f**) = 2 Å.

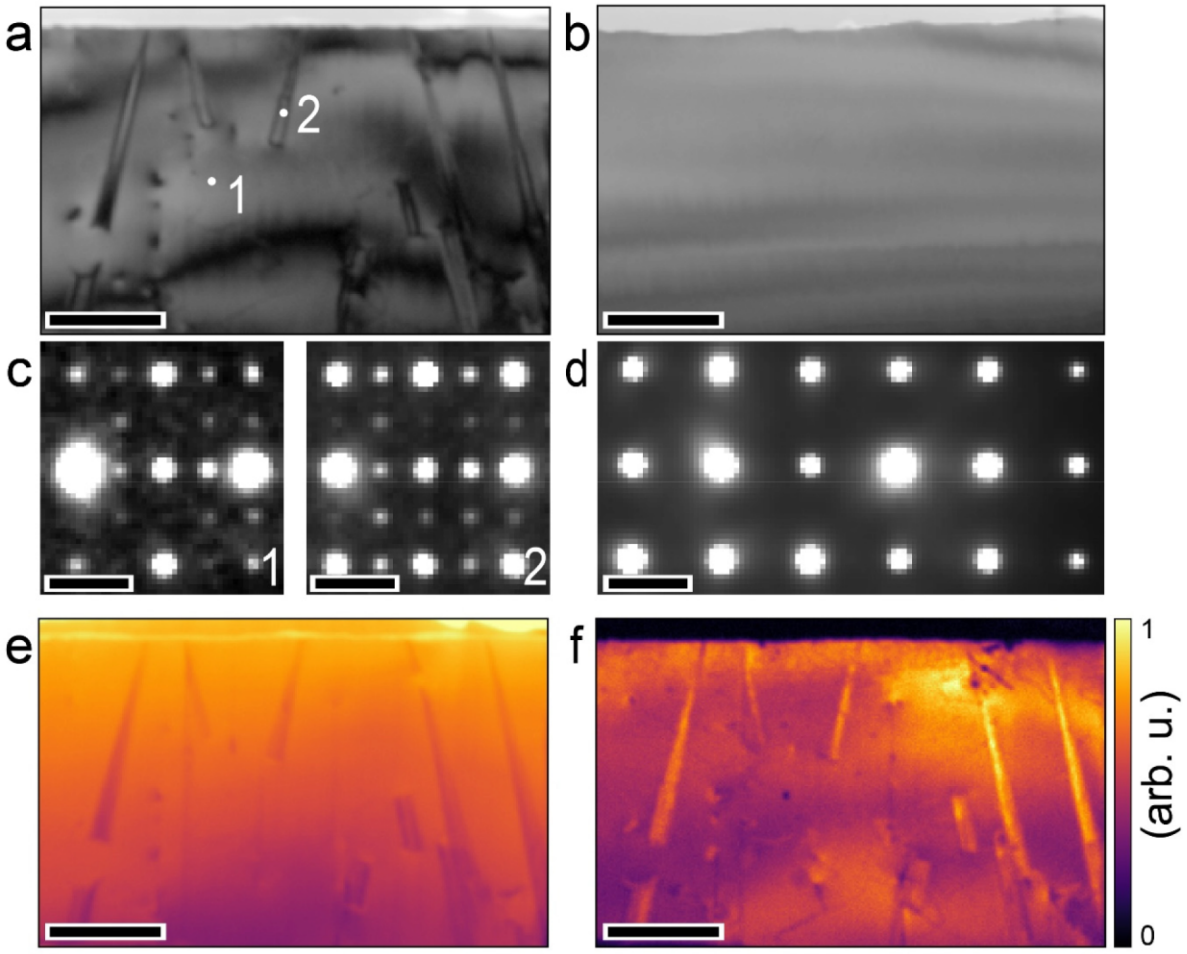

Figure 2: Virtual bright-field STEM images of **(a)** 320°C and **(b)** 560°C annealed samples reconstructed from 4D-STEM data collected at 100 K. **c.** Diffraction patterns from two probe positions in the 320°C sample – CDW peaks are stronger at the defect. **d.** Summed diffraction pattern from the 560°C sample showing no CDW peaks. Real-space maps of 320°C annealed sample, generated by selecting **(e)** Bragg peaks and **(f)** CDW peaks. Scale bars for (**a, b, e, f**) = 1 μm; for (**c, d**) = 2 nm^{-1}.

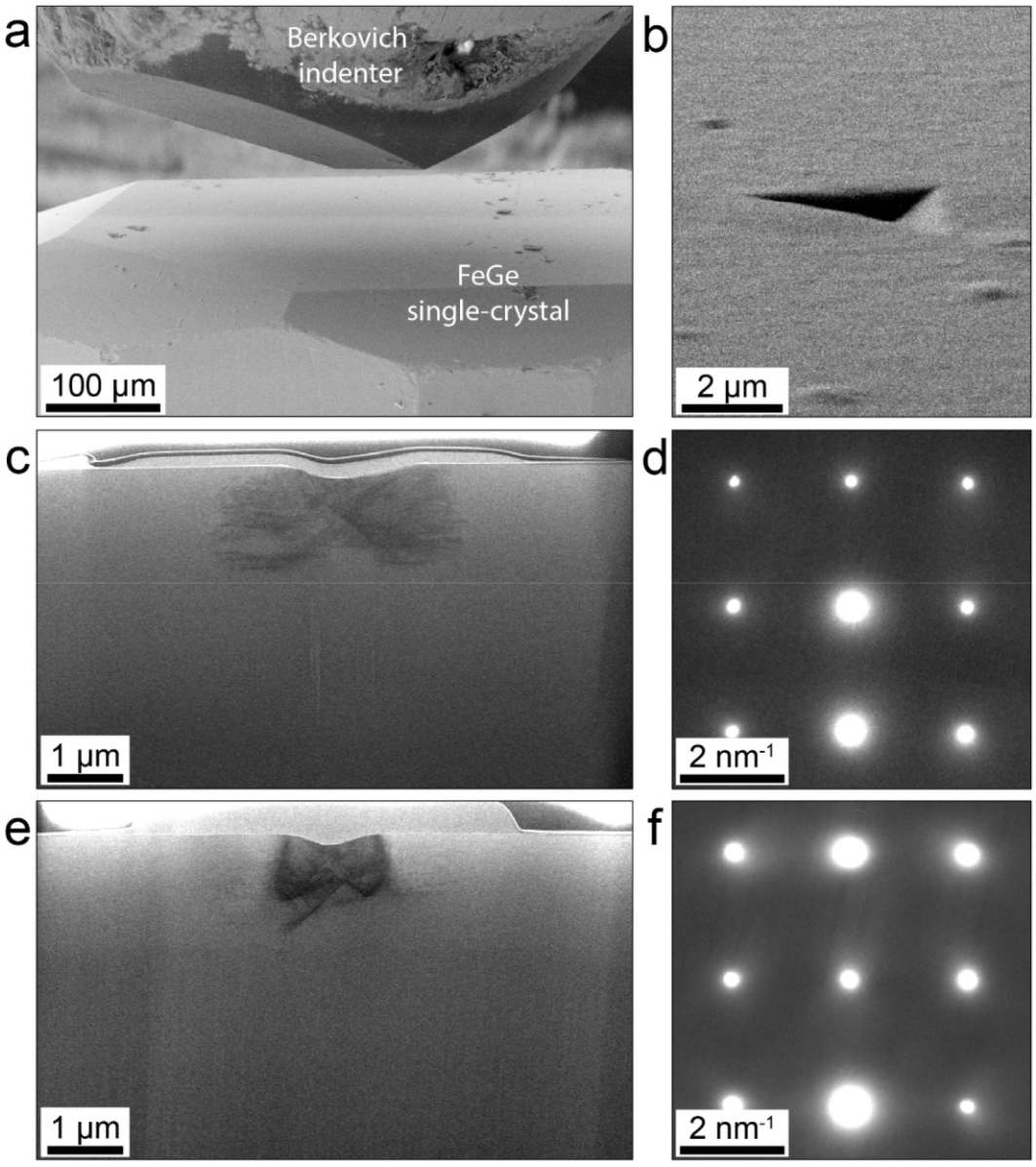

Figure 3: **a.** SEM image of *in situ* nanoindentation of as-grown and 560°C annealed samples with a Berkovich tip. **b.** SEM image of an indent of depth ~250 nm. **c.** ABF-STEM image of as-grown FeGe showing dislocations near the indentation. **d.** SAED pattern of indented, as-grown FeGe at 100 K showing no CDW satellite peaks. **e.** ABF-STEM of indented, 560°C annealed FeGe and **(f)** its SAED pattern at 100 K.

References

1. G Grüner, *Rev. Mod. Phys.* (1988) **60**, 1129
2. A Gabovich *et al. Supercond. Sci. Technol.* (2001) **14**, R1
3. X Teng *et al. Nature* (2022) **609**, 490-495
4. X Wu *et al. Phys. Rev. Lett.* (2024) **132**, 256501
5. Z Chen *et al. Nature Commun.* (2024) **15**, 6262
6. M Klemm *et al. arXiv*:2410.13994 (2024)
7. A Berghezan *et al. Acta Metallurgica* (1961) **9**, 464-491
8. Tokura *et al. Nature* (1989) **337**, 345-347
9. Wu *et al. Nature Commun.* (2024) **15**, 2739
10. The authors acknowledge funding from the DOE, Basic Energy Sciences program (grant DE-SC0023905). This work made use of shared facilities at Cornell: CCMR and PARADIM (DMR-2039380).